scientific reports

Check for updates

OPEN

Bimetallic Fe/K γ-cyclodextrin metal–organic frameworks with enhanced loading capacity and tunable release behavior

Asma Sadeghi[1], Hamidreza Farnoush[1]✉, Javad Safaei-ghomi[2]✉ & Hourieh Sadat Oboudatian[2]

Cyclodextrin-based metal–organic frameworks (CD-MOFs) are bio-derived porous coordination materials that combine hierarchical porosity with intrinsic host–guest recognition. Here, we report the synthesis of a bimetallic γ-cyclodextrin metal–organic framework incorporating potassium and iron ions (Fe/K-CD-MOF) via a controlled vapor diffusion method and examine the influence of dual-metal coordination on structural organization and guest transport behavior. Structural characterization by Fourier-transform infrared spectroscopy, powder X-ray diffraction, scanning and transmission electron microscopy, energy-dispersive X-ray spectroscopy, and Brunauer–Emmett–Teller analysis confirmed preservation of the γ-cyclodextrin framework together with improved crystallographic ordering and increased accessible surface area following iron incorporation. Curcumin was used as a model hydrophobic guest molecule to evaluate encapsulation efficiency and host–guest interactions. The Fe/K-CD-MOF exhibited higher loading capacity than the monometallic analogue, which is attributed to modified coordination environments and enhanced pore accessibility arising from heterometallic crosslinking. Release studies conducted under acidic and neutral conditions demonstrated pH-responsive behavior, indicating diffusion-controlled transport influenced by framework–guest interactions. Kinetic modeling using Freundlich, Ritger–Peppas, and Elovich equations suggested a combined adsorption–diffusion mechanism with anomalous transport characteristics. These findings establish a direct relationship between bimetallic coordination and functional performance in γ-cyclodextrin MOFs, providing a rational strategy for tuning carbohydrate-based porous materials for controlled molecular delivery.

Keywords γ-cyclodextrin metal–organic framework, Bimetallic coordination, Host–guest interactions, PH-responsive release, Porous biomaterials

The rational design of porous coordination materials has become a central theme in materials chemistry due to their tunable architectures, high surface areas, and capacity for controlled molecular transport[1,2]. Among these materials, metal–organic frameworks (MOFs) have attracted sustained attention because their crystalline networks are constructed from metal nodes and multitopic organic ligands linked through well-defined coordination geometries[3,4]. The modular nature of metal–ligand assembly allows systematic control over pore size distribution, surface chemistry, and framework stability. Consequently, MOFs provide a versatile platform for investigating adsorption thermodynamics, molecular confinement, and diffusion-controlled transport phenomena in structured porous environments[5–7]. The physicochemical behavior of MOFs is intrinsically governed by the identity of the metal centers and their coordination environment[8,9]. Parameters such as ionic radius, charge density, preferred coordination number, ligand field effects, and metal–oxygen bond strength influence network topology and long-range crystallographic ordering[9]. Variations in these parameters alter crosslinking density, pore accessibility, and structural rigidity, ultimately determining adsorption capacity and guest mobility. Therefore, deliberate modulation of metal–ligand interactions represents a powerful strategy for tailoring MOF functionality through coordination chemistry.

[1]Department of Metallurgy and Materials Engineering, Faculty of Engineering, University of Kashan, Kashan 87317-51167, Iran. [2]Department of Organic Chemistry, Faculty of Chemistry, University of Kashan, Kashan 51167, I.R. of Iran. ✉email: farnoush@kashanu.ac.ir; safaei@kashanu.ac.ir

In parallel with advances in synthetic MOF chemistry, increasing emphasis has been placed on the development of bio-derived frameworks that combine structural tunability with biocompatibility and sustainability[10]. Cyclodextrins (CDs), cyclic oligosaccharides composed of α-(1→4)-linked glucopyranose units, have emerged as attractive building blocks for such systems[11]. Their truncated cone geometry provides a hydrophobic internal cavity capable of forming inclusion complexes with diverse guest molecules, while the exterior surface is rich in hydroxyl groups that can participate in hydrogen bonding and metal coordination. This dual functionality enables cyclodextrins to serve both as supramolecular hosts and as multidentate ligands in coordination assemblies[12]. Among the cyclodextrin homologues, γ-cyclodextrin (γ-CD) consists of eight glucopyranose units and offers a relatively large toroidal cavity along with multiple primary hydroxyl groups arranged at the narrower rim[12,13]. These hydroxyl groups can coordinate alkali metal ions, promoting the formation of extended three-dimensional networks through metal-mediated bridging interactions. The resulting cyclodextrin-based MOFs (CD-MOFs) possess hierarchical porosity derived from both intrinsic γ-CD cavities and interstitial channels generated during framework assembly[14–19]. In conventional γ-CD-MOFs, potassium ions (K^+) act as primary coordination centers, forming ionic interactions with deprotonated hydroxyl groups and stabilizing the cubic crystalline architecture[20].

Although monometallic γ-CD-MOFs have been widely investigated for adsorption, encapsulation, and delivery applications, the coordination environment in these systems is predominantly defined by monovalent alkali metal ions[21]. Such ions typically exhibit flexible coordination geometries and relatively weak, electrostatically dominated metal–oxygen interactions. As a result, framework stability and crosslinking density are largely controlled by ionic association rather than directional bonding. While this configuration preserves the intrinsic γ-CD cavity and allows efficient inclusion, it may limit the degree of structural reinforcement and restrict opportunities for fine-tuning pore architecture.

Incorporation of a secondary metal species introduces an additional level of coordination complexity that may significantly influence network connectivity and structural ordering[22–24]. Transition metal ions, such as Fe^{3+}, differ substantially from alkali metals in terms of valence state, charge density, and preferred coordination geometry[11]. The higher positive charge and smaller ionic radius of Fe^{3+} confer stronger and more directional metal–oxygen interactions with hydroxyl groups. Moreover, Fe^{3+} commonly adopts octahedral coordination geometries, potentially acting as multidentate crosslinking nodes that increase framework rigidity and modify pore connectivity. Such heterometallic coordination could enhance long-range crystallographic ordering, alter electronic distribution within the network, and influence surface accessibility without disrupting the fundamental toroidal structure of γ-CD.

Despite these theoretical considerations, systematic experimental investigations correlating heterometallic coordination with structural and functional properties in γ-CD-MOFs remain limited. In particular, direct relationships between dual-metal coordination, surface area modulation, and guest transport dynamics have not been comprehensively established. Understanding these correlations is essential for developing rational design strategies that exploit coordination chemistry to control framework performance. Iron was selected as the secondary metal ion due to its unique combination of coordination versatility, environmental compatibility, and functional performance in host–guest systems[25]. From a coordination chemistry perspective, Fe^{3+} exhibits strong affinity toward oxygen-containing ligands, such as the hydroxyl groups of γ-cyclodextrin, enabling the formation of stable and well-defined metal–organic frameworks. Compared to divalent cations (e.g., Zn^{2+} or Mg^{2+}), Fe^{3+} provides higher charge density, which enhances framework stability and crosslinking density[26]. From a biomedical and environmental standpoint, iron is inherently biocompatible, non-toxic at controlled levels, and widely used in drug delivery and biomedical applications[27]. This makes Fe-based CD-MOFs particularly attractive for controlled release systems compared to heavier or toxic metals (e.g., Cu^{2+}, Co^{2+}). Moreover, the redox-active nature of iron (Fe^{2+}/Fe^{3+}) introduces additional functionality, enabling tunable interactions with guest molecules and potentially influencing release kinetics through coordination strength modulation[28]. This redox flexibility distinguishes iron from other multivalent cations such as Al^{3+}, which lack similar electronic adaptability. Therefore, Fe was selected as an optimal candidate to simultaneously enhance structural stability, improve host–guest interactions, and maintain biocompatibility, making it superior to many alternative metal ions for γ-CD-MOF design.

To probe structure–property relationships in heterometallic γ-CD-MOFs, a suitable guest molecule is required that is sensitive to confinement effects and transport limitations. Curcumin, a naturally occurring polyphenolic compound isolated from Curcuma longa, provides an appropriate molecular probe. Its conjugated diketone structure enables keto–enol tautomerism and metal chelation, while its hydrophobic character and low aqueous solubility render it poorly dispersible in polar media[29]. These characteristics make curcumin highly responsive to changes in pore environment and surface chemistry. Furthermore, its instability in aqueous conditions allows evaluation of diffusion-controlled release processes and framework–guest interactions[30–33]. Accordingly, curcumin serves as a representative model for assessing encapsulation efficiency and transport behavior in porous coordination materials. In this study, mono- and bimetallic γ-CD-MOFs incorporating potassium and iron ions were synthesized via a controlled vapor diffusion method to elucidate the influence of dual-metal coordination on framework architecture. The introduction of Fe^{3+} alongside K^+ was hypothesized to increase crosslinking density and modify pore accessibility through stronger and more directional metal–oxygen bonding interactions. The resulting Fe/K-CD-MOF exhibited a BET surface area of 345.4 $m^2\ g^{-1}$, approximately 15% higher than the monometallic K-CD-MOF (298.7 $m^2\ g^{-1}$), along with a reduced average particle size of ~ 420 nm and enhanced crystallinity as evidenced by low-angle XRD reflections at 7.1°, 12.24°, and 13.19°. Comprehensive structural characterization was conducted using vibrational spectroscopy, powder X-ray diffraction, scanning and transmission electron microscopy, elemental mapping, and Brunauer–Emmett–Teller surface area analysis to establish correlations between coordination environment, crystallinity, morphology, and porosity. Curcumin was subsequently employed to evaluate host–guest functionality through encapsulation efficiency

measurements and pH-responsive release studies under acidic and neutral conditions. Kinetic modeling was applied to distinguish adsorption-dominated processes from diffusion-controlled transport mechanisms within the modified framework. By integrating coordination chemistry principles with adsorption and release analysis, this work aims to clarify how heterometallic modulation influences both structural organization and functional performance in carbohydrate-based MOFs. The results demonstrate that incorporation of Fe^{3+} into the γ-CD framework enhances long-range ordering and surface accessibility, leading to improved guest loading and tunable release behavior. These findings establish a direct structure–property relationship in bimetallic γ-CD-MOFs and highlight heterometallic coordination as an effective strategy for engineering tunable bio-derived porous materials. The insights gained provide a foundation for extending coordination-based modulation approaches to other carbohydrate-derived frameworks and controlled molecular delivery systems.

Experimental

Materials and methods

Potassium acetate (CH_3COOK), gamma-cyclodextrin ($C_{48}H_{80}O_{40}$), iron(II) sulfate ($FeSO_4{\cdot}7\ H_2O$), curcumin ($C_{21}H_{20}O_6$), sodium acetate (CH_3COONa), potassium chloride (KCl), potassium dihydrogen phosphate (KH_2PO_4), and dipotassium hydrogen phosphate (K_2HPO_4) were purchased from Sigma-Aldrich or Merck Companies. Also, methanol (CH_3OH), absolute ethanol (C_2H_5OH), dimethylformamide (C_3H_7NO), acetone (C_3H_6O), acetic acid (CH_3COOH), and hydrochloric acid (HCl, 37%) were purchased from Merck and Sigma-Aldrich Companies. All materials were analytical grade and used as received without further purification.

The evolution of the MOF structure was monitored with FTIR on a Nicolet Magna 550 using KBr pellets. TEM (Zeiss EM10C, Germany), operated at 100 kV, was used to analyze nanoparticle size and morphology. Nanoparticles were also analyzed with MIRA 3 TESCAN FE-SEM. Elemental analysis was done with EDX using a ZEISS Sigma with Oxford Instruments EDX. Textural properties (surface area) were measured using the BET method on nitrogen adsorption data from a Micromeritics Tristar 3000. Crystalline structure was characterized by powder XRD on a Philips X'Pert diffractometer. Quantitative determination of potassium and iron content in the bimetallic Fe/K-CD-MOF was performed using inductively coupled plasma mass spectrometry (ICP-MS). Approximately 10 mg of dried sample was digested in 2 mL of concentrated HNO_3 (69%) at 120 °C for 4 h, followed by dilution to 25 mL with ultrapure water (18.2 MΩ·cm). Measurements were conducted on an Agilent 8900 ICP-MS Triple Quadrupole system equipped with a MicroMist nebulizer and helium collision cell. Operating parameters were: RF power 1550 W, plasma gas flow 15.0 L min^{-1}, nebulizer gas flow 0.90 L min^{-1}, and He cell gas flow 5.0 mL min^{-1}. Calibration was performed using six standard solutions in the concentration range of 0.1–100.0 μg L^{-1} prepared from certified reference material (HPS, ICP-MS-68 A, traceable to NIST SRM 3100). Internal standard solution (10 μg L^{-1}, Agilent) was used for system stability control. Data processing and collection were performed using MassHunter workstation software. Each sample was analyzed in triplicate, and results are reported as mean ± standard deviation.

Synthetic methods

Preparation of porous K/Fe-CD-MOF

50 mg (0.9 mmol) of potassium acetate (CH_3COOK) and 100 mg (0.1 mmol) of iron(II) sulfate heptahydrate ($FeSO_4{\cdot}7\ H_2O$) were dissolved in deionized water. The mixture was stirred for 3 h at room temperature. Then, a solution of γ-cyclodextrin (260 mg, 0.2 mmol) in deionized water (6 mL) was slowly and dropwise added to the aqueous suspension and stirred for 8 h at room temperature (Fig. 1 (a)).

The resulting solution was then filtered through a 0.45 μm microporous membrane. The beaker was then transferred to a tank containing 50 mL of methanol, followed by methanol diffusion at room temperature for 7 days. K/Fe-CD-MOF was obtained by the modified vapor diffusion method, which has been previously reported[14,18,19,34,35]. In this method, the preferential volatilization of methanol may be directly introduced into a

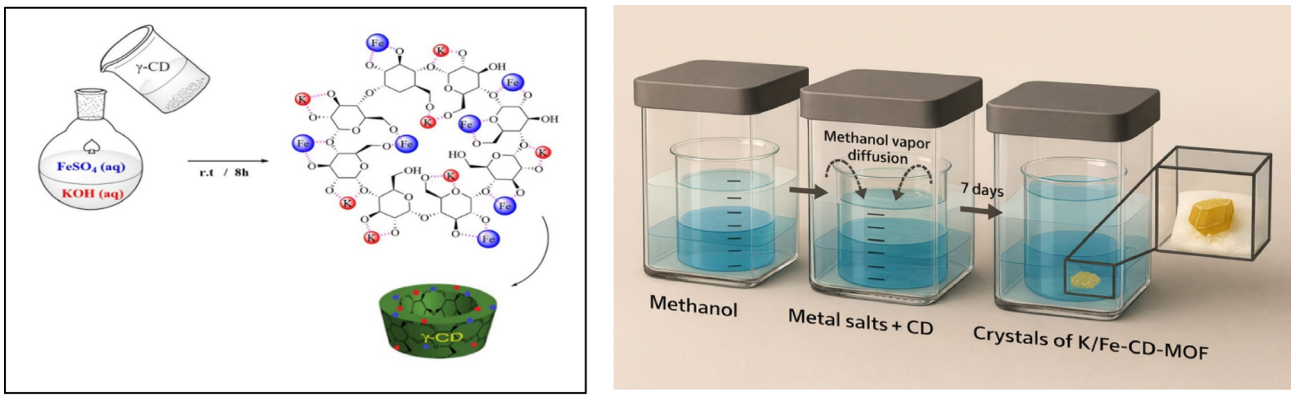


Fig. 1. Schematic illustration of **a** the preparation process of the bimetallic Fe/K-γ-CD-MOF and **b** the vapor diffusion method employed for the synthesis of γ-CD-based MOFs.

polar solution containing metals and organic linkers and generally reduces the solubility of the sample, leading to the slow formation of K/Fe-CD-MOF crystals[36]. After that, the solid product was filtered and washed three times with methanol to remove residual solvent and to open the pores of the MOF. The resulting K/Fe-MOF was dried at 35 °C in a vacuum oven for 8 h. Figure 1 (b) shows a schematic of the vapor diffusion method for the synthesis of K/Fe-CD-MOF crystals in methanol.

Preparation of K-CD- MOF

897 mg (1.6 mmol) of potassium acetate and 260 mg (0.2 mmol) of γ-cyclodextrin were dissolved in 4 mL of deionized water and stirred for 8 h at 70 °C. Afterward, the solution was filtered through a 0.45 µm syringe filter. The beaker was then transferred to a tank containing 50 mL of methanol, followed by methanol diffusion at room temperature for 7 days. The products were carefully separated from the solution and washed three times with methanol. Finally, the colorless crystals were dried in a vacuum oven at 35 °C for 8 h and ground to fine powders for subsequent applications.

Preparation of Fe-CD-MOF

For the synthesis of Fe-CD-MOF, all the reaction conditions were similar to those of K-CD-MOF, except for changing the potassium acetate to iron(II) sulfate heptahydrate ($FeSO_4{\cdot}7\ H_2O$) (55 mg, 0.4 mmol). During the synthesis, although $FeSO_4{\bullet}7\ H_2O$ was used as the iron precursor (Fe^{2+} source), partial oxidation of Fe^{2+} to Fe^{3+} is expected under the employed conditions[37]. The reaction was carried out in aqueous medium under ambient atmosphere and prolonged stirring (≈ 11 h total), followed by slow methanol vapor diffusion over 7 days. Under these conditions, dissolved oxygen promotes oxidation of Fe^{2+} according to[38]:

$$4Fe^{2+} + O_2 + 2H_2O \rightarrow 4Fe^{3+} + 4OH^- \quad (1)$$

In addition, the coordination environment provided by γ-cyclodextrin (rich in hydroxyl groups) stabilizes Fe^{3+} through stronger metal–ligand interactions compared to Fe^{2+}. Therefore, the final framework is expected to predominantly contain Fe^{3+} species, with possible minor residual Fe^{2+} depending on local coordination environments.

Loading of curcumin

An amount of 200 mg of curcumin was dissolved in 15 mL of methanol. To this mixture, 100 mg of X-MOF was added drop wise with stirring at room temperature; temperature was protected from light (25 °C). To quantitatively measure drug loading, three 500 µl aliquots from the mixture were taken at 24, 48 and 96 h, with each sample measured for curcumin concentration using UV-Vis spectroscopy at 425 nm. After 96 h, the loaded MOFs were centrifuged and washed two times with methanol. The solid product was then dried at 37 °C for 24 h.

Curcumin release studies

The curcumin release behavior from the nanocarriers was assessed through in vitro release studies. The studies were done at two different pH levels (2.0 and 7.4), which represent acidic and neutral buffer environments commonly used to study pH-dependent release behavior. To carry out the release study, 1 mg of the curcumin-loaded nanocarrier in a 30 mL buffer solution (at 37 °C) were placed in a flask with a stirring rod. The flask was placed in a light-protective container during the release study. At various times during the study (0.5, 1, 2, 3, 4, 8, 12, and 24 h) a sample of the solutions was removed and the concentration of the released curcumin was determined by UV-Vis spectroscopy at 425 nm. Each curcumin-loaded nanocarrier was subjected to the testing at pH 2.0 (using a standard KCl/HCl buffer solution) and pH 7.4 (using a phosphoric acid-buffered system).

Results and discussion

FT-IR analysis

The FT-IR spectra of (a) γ-cyclodextrin (γ-CD), (b) K-CD-MOF, (c) Fe-CD-MOF, and (d) Fe/K-CD-MOF are shown in Fig. 2. Pristine γ-CD (Fig. 2a) exhibits a broad absorption band centered at 3309 cm^{-1}, corresponding to the stretching vibration of hydroxyl (–OH) groups involved in extensive intermolecular hydrogen bonding, a characteristic feature of polysaccharide-based macromolecules. The weak band at approximately 2923 cm^{-1} is attributed to aliphatic C–H stretching vibrations of the glucopyranose units. The characteristic absorptions at 1022 and 1152 cm^{-1} correspond to C–O and C–O–C stretching vibrations, respectively, confirming the integrity of the cyclodextrin backbone. The band observed at ~1641 cm^{-1} is associated with the bending vibration of adsorbed water molecules, while the signal around 575 cm^{-1} arises from skeletal vibrations of the polysaccharide framework.

Upon coordination with metal ions, noticeable spectral changes are observed for all CD-MOF samples. Deconvolution of the O–H stretching region (3300–3500 cm^{-1}) reveals three component bands corresponding to free O–H (~3450 cm^{-1}), hydrogen-bonded O–H (~3350 cm^{-1}), and metal-coordinated O–H (~3250 cm^{-1}). The relative area of the metal-coordinated band increases from 12% in K-CD-MOF to 18% in Fe/K-CD-MOF, indicating a higher degree of metal–oxygen coordination in the bimetallic system. The observed shifts in C–O stretching bands (from 1022 cm^{-1} in γ-CD to 1015 cm^{-1} in Fe/K-CD-MOF) are consistent with literature reports of metal coordination to cyclodextrin hydroxyl groups[11].

Notably, the bimetallic Fe/K-CD-MOF (Fig. 2d) displays sharper and split bands at approximately 580 and 523 cm^{-1} compared to the monometallic counterparts, reflecting the presence of distinct metal–oxygen coordination environments. The selection of Fe as a co-metal is justified by its strong coordination with hydroxyl groups, high biocompatibility, and redox flexibility (Fe^{2+}/Fe^{3+}), which collectively enhance framework stability and guest–host interactions compared to conventional divalent or non-redox-active cations. In addition,

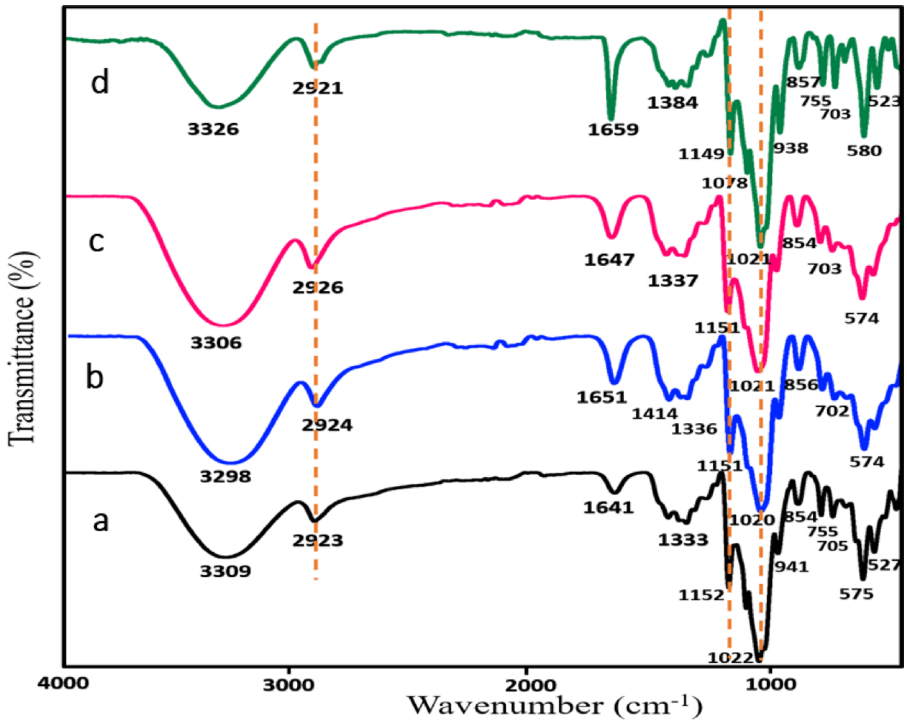


Fig. 2. FT-IR spectra of **a** γ-CD, **b** K-CD-MOF, **c** Fe-CD-MOF, and **d** Fe/K-CD-MOF.

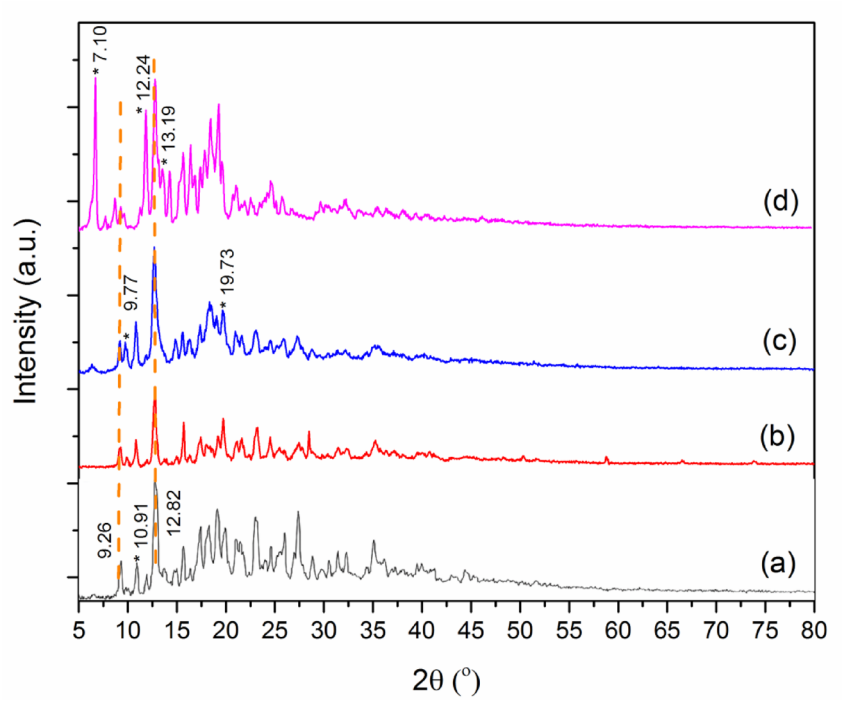
the band near 1659 cm^{-1} becomes sharper and shifts to higher wavenumbers, indicating reduced structural water content and a more ordered hydrogen-bonding network. These observations confirm the successful formation of a bimetallic γ-CD-based coordination framework with enhanced structural organization relative to monometallic systems[39].

Powder-X-ray diffraction analysis

The powder XRD patterns of γ-CD, K-CD-MOF, Fe-CD-MOF, and Fe/K-CD-MOF are presented in Fig. 3. Pristine γ-CD exhibits characteristic diffraction peaks at 2θ values of approximately 9.26°, 10.91°, and 12.82°, which are considered fingerprint reflections of its crystalline supramolecular arrangement. Coordination with K^+ or Fe^{2+}/Fe^{3+} ions leads to peak shifts and broadening, indicating partial modulation of the native γ-CD lattice while preserving its fundamental framework. Comparison of the experimental patterns with literature reports of γ-CD-MOFs[40] confirms retention of the characteristic cubic framework topology. The low-angle reflection at approximately 7.1° corresponds to the (200) plane of the cubic unit cell, consistent with reported values. The absence of reflections that would indicate framework collapse or formation of a different crystalline phase supports the conclusion that the γ-cyclodextrin scaffold remains intact after metal coordination.

The oxidation state of iron in the synthesized K/Fe–CD–MOF requires careful consideration, as $FeSO_4 \cdot 7\ H_2O$ introduces Fe^{2+} initially. However, under ambient aqueous conditions and prolonged synthesis time, Fe^{2+} is thermodynamically unstable and readily oxidizes to Fe^{3+} in the presence of dissolved oxygen. This transformation is further facilitated by the strong coordination ability of γ-cyclodextrin hydroxyl groups, which preferentially stabilize Fe^{3+} centers due to their higher charge density and stronger ligand field interactions. Previous studies on cyclodextrin-based MOFs and related aqueous Fe systems have consistently reported spontaneous oxidation of Fe^{2+} to Fe^{3+} during synthesis under similar conditions. Consequently, the dominant oxidation state of iron in the final framework is assigned to Fe^{3+}, although partial coexistence of Fe^{2+}/Fe^{3+} redox pairs cannot be completely excluded. This mixed-valence scenario may also contribute to enhanced coordination flexibility and improved functional performance of the framework.

For K-CD-MOF (Fig. 3b), the disappearance of reflections at 11.19° and 20.18° suggests successful incorporation of potassium ions within the cyclodextrin framework. In Fe-CD-MOF (Fig. 3c), the emergence of new reflections near 9.77° and 13.73°, along with intensity redistribution, reflects iron-induced structural rearrangements. In contrast, the bimetallic Fe/K-CD-MOF (Fig. 3d) exhibits sharper and more intense diffraction peaks, including prominent reflections at 7.1°, 12.24°, 12.83°, and 13.19°, as well as an increased density of peaks in the 15–22° range. These features indicate enhanced crystallinity and improved long-range ordering resulting from cooperative bimetal coordination. The intense low-angle reflection at 7.1° is suggestive of increased interlayer spacing, which may be associated with the formation of a bimetallic coordination network. However, we acknowledge that definitive assignment of lattice parameters would require Rietveld refinement against higher-resolution synchrotron XRD data. Therefore, while the data indicate improved crystallographic ordering in the bimetallic system, statements about specific lattice dimensions remain preliminary. Low-angle XRD analysis (Fig. 3e) further confirms this ordering, with distinct reflections at 6.2° and 8.5°. Overall, the data



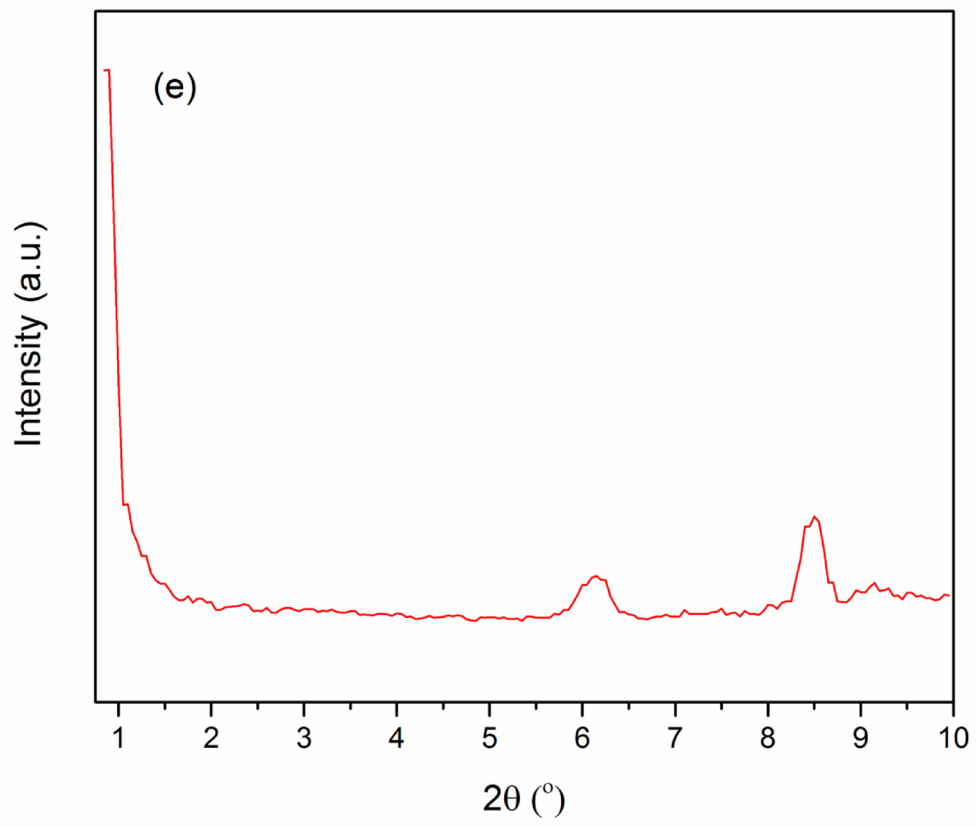


Fig. 3. XRD patterns of **a** γ-CD, **b** K-CD-MOF, **c** Fe-CD-MOF, **d** Fe/K-CD-MOF, and **e** low-angle XRD pattern of Fe/K-CD-MOF.

indicate that while the cyclodextrin macromolecular framework remains intact, bimetallic Fe/K coordination promotes superior supramolecular organization, consistent with FT-IR observations[41].

SEM and TEM analysis

The morphology of the synthesized CD-MOFs was examined by SEM (Fig. 4). Monometallic K-CD-MOF and Fe-CD-MOF (Fig. 4b and c) consist of relatively larger, aggregated particles. In contrast, the bimetallic Fe/K-CD-MOF (Fig. 4a) exhibits a more homogeneous morphology with a reduced average particle size of approximately 420 nm. The smaller and more uniform particles in the bimetallic system are attributed to cooperative nucleation effects arising from simultaneous Fe and K coordination, which suppress excessive crystal growth. These observations are consistent with the enhanced crystallinity observed in XRD analysis.

TEM images of Fe/K-CD-MOF (Fig. 4d, e) reveal aggregated nanoscale domains with distinct contrast variations. Darker regions correspond to metal-rich coordination domains, while lighter regions represent the cyclodextrin-based organic matrix. This contrast confirms the formation of an integrated bimetallic coordination network within the macromolecular scaffold.

Elemental composition analysis

The identification and analysis of the elemental composition and relative abundance of the constituent elements between the two types of nanoparticles was accomplished using energy-dispersive X-ray spectroscopy (EDS) and elemental mapping analyses on each of the two samples (i.e., the bimetallic Fe/K-MOF and monometallic K-MOF). The results provided in Fig. 5 indicate that there are iron, potassium, carbon, and oxygen present in the bimetallic Fe/K-MOF, while just potassium, carbon, and oxygen are present in the monometallic K-MOF. Figure 5a contains the corresponding weight and atomic amounts of each of the elements, as well as their spatial distributions and dispersions within the bimetallic Fe/K-MOF. The EDX analysis of the monometallic K-MOF

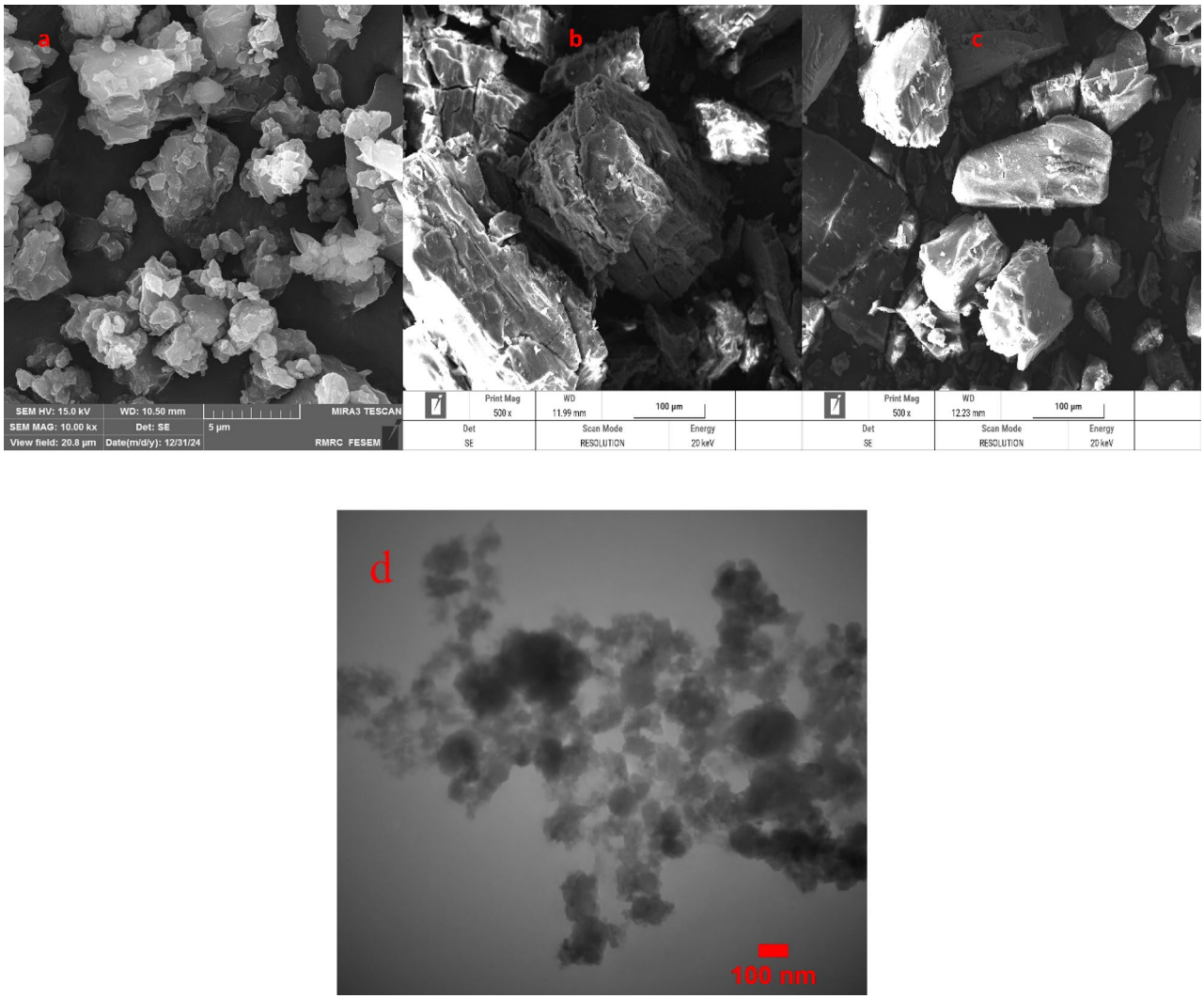
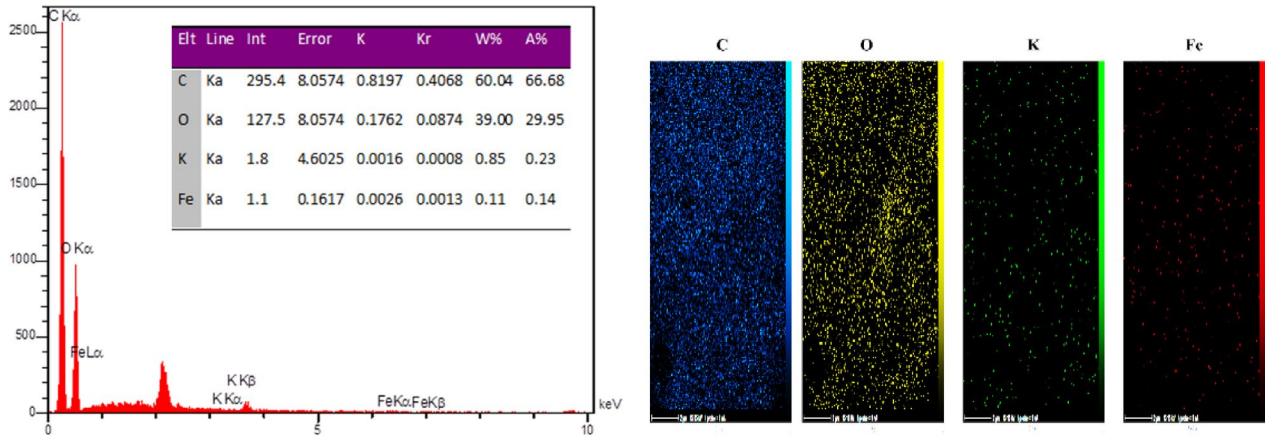
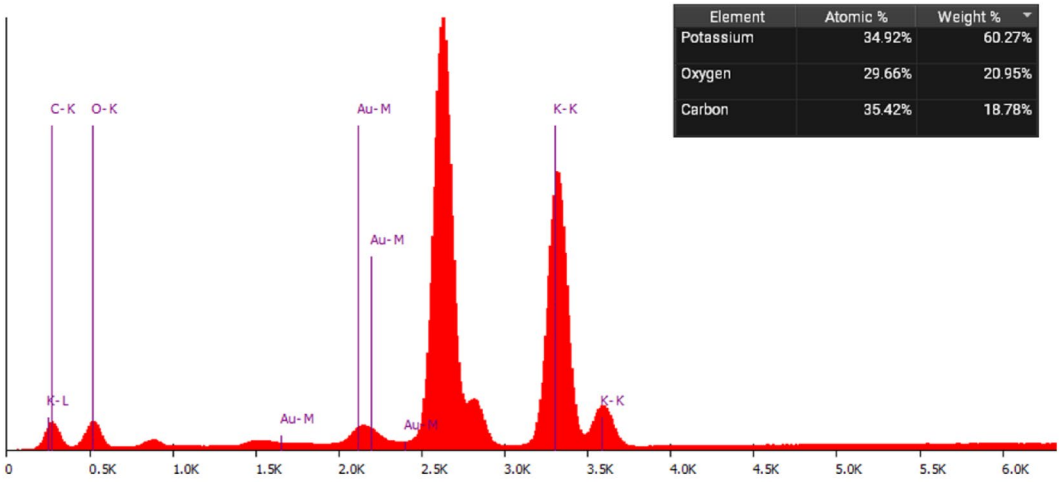


Fig. 4. SEM images of **a** Fe/K-CD-MOF, **b** K-CD-MOF, and **c** Fe-CD-MOF; **d**, **e** TEM images of Fe/K-CD-MOF.



(a)



(b)

Fig. 5. **a** EDS spectrum and elemental mapping of Fe/K-CD-MOF, and **b** EDS spectrum of K-CD-MOF.

shows a relatively high percentage of potassium due to the monometallic system. Conversely, the bimetallic Fe/K-MOF showed lower metal content overall (Fe and K) due to the coordination of metal ions within cyclodextrin. The elemental mapping data show a uniform distribution of Fe and K throughout the sample, with no evidence of iron oxide clusters or separate iron-containing phases. This uniform distribution suggests that iron is incorporated into the framework coordination nodes rather than being merely surface-deposited or present as a separate phase. The absence of phase segregation confirms that a well-dispersed bimetallic coordination network was formed, where Fe^{3+} and K^{+} ions cooperatively participate in crosslinking the γ-cyclodextrin ligands.

To obtain quantitative metal content, the bimetallic Fe/K-CD-MOF was further analyzed by ICP-MS. The measured potassium content was 0.90 ± 0.05 mg g^{-1} (0.0230 ± 0.0013 mmol g^{-1}), and the total iron content was 0.17 ± 0.02 mg g^{-1} (0.0030 ± 0.0004 mmol g^{-1}). Based on the γ-cyclodextrin content in the framework, the calculated molar ratios are approximately γ-CD : K : Fe = 1 : 4.6 : 0.6. The Fe/K molar ratio is 0.13, confirming the successful incorporation of iron at approximately one-sixth the molar amount of potassium. This relatively low iron content is consistent with the role of Fe^{3+} as a secondary crosslinking agent that enhances framework stability without disrupting the primary K^{+}-based coordination network. The observed Fe/K ratio is also consistent with the synthesis feed ratio (0.1 mmol Fe : 0.9 mmol K = 0.11), indicating efficient incorporation of both metals with minimal loss during washing.

To assess the oxidation state distribution, a separate aliquot was analyzed after reduction with hydroxylamine hydrochloride to determine total iron, and the difference between total iron and Fe^{2+} (determined by 1,10-phenanthroline colorimetry) gave the Fe^{3+} content. Approximately 90% of the incorporated iron was present as Fe^{3+} (0.15 ± 0.02 mg g^{-1}), with the remainder as Fe^{2+} (0.02 ± 0.01 mg g^{-1}). This confirms that partial

oxidation of Fe^{2+} to Fe^{3+} occurred during synthesis, consistent with the experimental clarification in the section "Preparation of Fe-CD-MOF". The predominance of Fe^{3+} is advantageous for framework stability due to its higher charge density and stronger coordination with cyclodextrin hydroxyl groups. Despite these findings, several limitations should be acknowledged. The precise oxidation state and coordination environment of iron were not directly determined, and advanced spectroscopic techniques would provide further insight. In addition, quantitative elemental analysis and systematic variation of Fe/K ratios were beyond the scope of this study but represent important directions for future work.

BET analysis

The textural properties of the synthesized MOFs were evaluated by nitrogen adsorption–desorption measurements. The N_2 sorption isotherms of K-MOF and Fe/K-MOF are shown in Fig. 6. The calculated BET surface areas are 298.7 $m^2\ g^{-1}$ for K-MOF and 345.4 $m^2\ g^{-1}$ for Fe/K-MOF, indicating that incorporation of Fe ions alongside K ions leads to an increase in accessible surface area. The total pore volumes, determined from the amount of N_2 adsorbed at $P/P_0 = 0.99$, were 1.50 $cm^3\ g^{-1}$ for K-MOF and 4.43 $cm^3\ g^{-1}$ for Fe/K-MOF. Pore size distribution analysis using the Barrett–Joyner–Halenda (BJH) method revealed a bimodal distribution for both samples, with micropores centered at approximately 0.8 nm and mesopores ranging from 2 to 5 nm. The bimetallic sample exhibited a higher proportion of mesopores, which likely contributes to its enhanced curcumin loading capacity and altered release behavior.

Both samples exhibit adsorption isotherms characteristic of a combination of type I and type IV behavior, accompanied by a narrow hysteresis loop in the relative pressure (P/P_0) range of 0.3–1.0. The steep uptake at low relative pressures suggests the presence of micropores, while the hysteresis loop at higher pressures indicates mesoporous characteristics. The coexistence of micro- and mesoporous structures is advantageous for drug loading and release, providing sufficient surface area as well as accessible pore channels for guest molecule diffusion.

Loading and release behavior of curcumin

Calibration curve and loading confirmation

A calibration curve for curcumin was established using UV–Vis spectroscopy at the characteristic absorption wavelength (425 nm), showing a good linear relationship between absorbance and concentration within the studied range (ESI Fig. S1). This calibration curve was used to quantify the amount of curcumin released from the carriers during the release experiments.

Structural characterization after drug loading

FT-IR and XRD analyses were performed to confirm the successful loading of curcumin onto the γ-CD, K-MOF, and Fe/K-MOF carriers. The FT-IR patterns of curcumin and other X-MOF@Cur carriers are shown in Fig. 7. The characteristic peaks of curcumin could be observed at 1626 cm^{-1}, representing stretching vibration of the carboxyl groups C = O. The peaks at 1425 and 1595 cm^{-1} can be assigned to the stretching vibration of the C = C bond in the aromatic ring. In addition, the peak at 3505 cm^{-1} is related to the O-H groups, and the peak at 1272 cm^{-1} corresponds to C–O vibration of phenol groups (Fig. 7a). As shown in Fig. 7 compared to Fig. 2, the

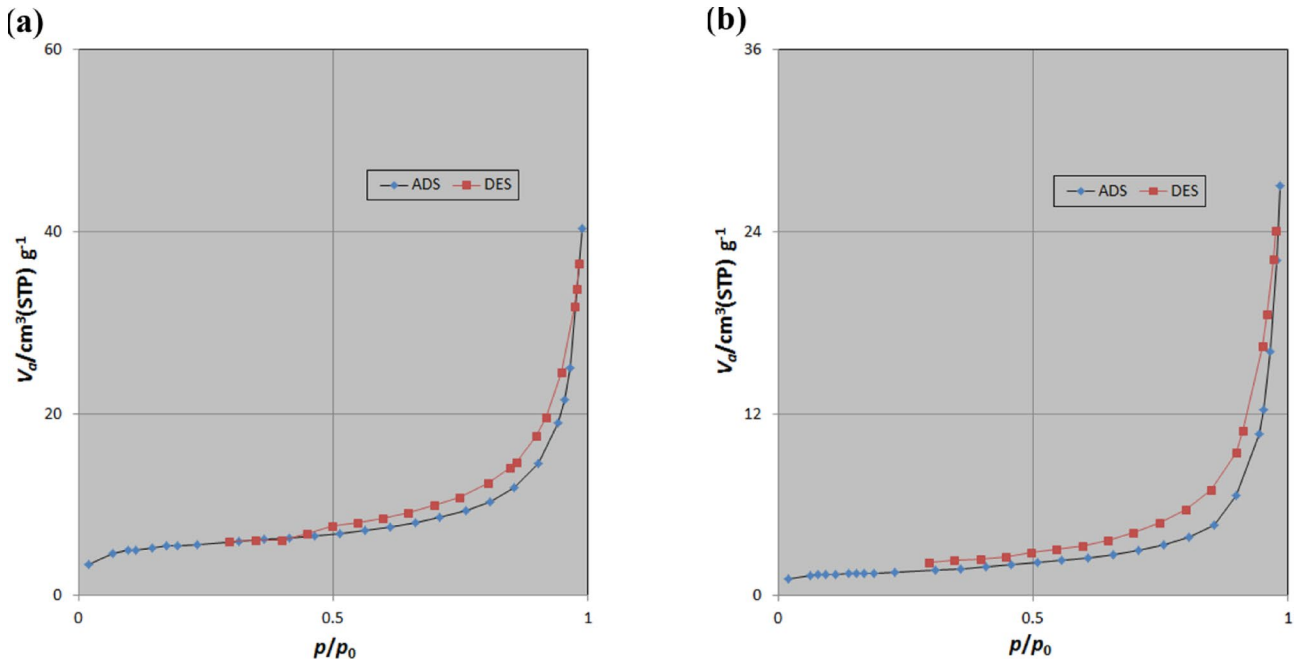


Fig. 6. BET nitrogen adsorption–desorption isotherms of **a** K-CD-MOF and **b** Fe/K-CD-MOF.

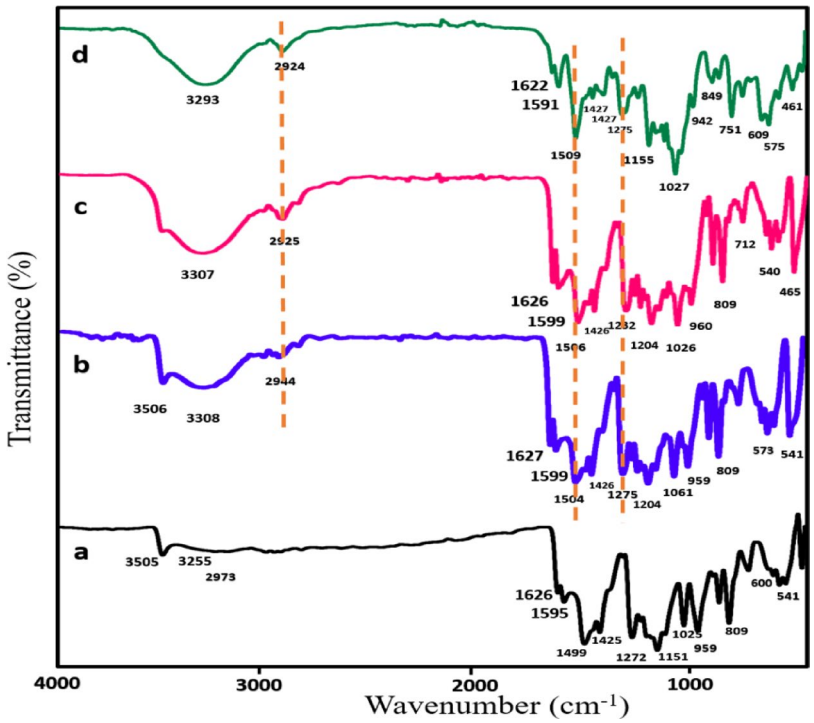


Fig. 7. FT-IR spectra of **a** curcumin, **b** K-CD-MOF@Cur, **c** Fe-CD-MOF@Cur, and **d** Fe/K-CD-MOF@Cur.

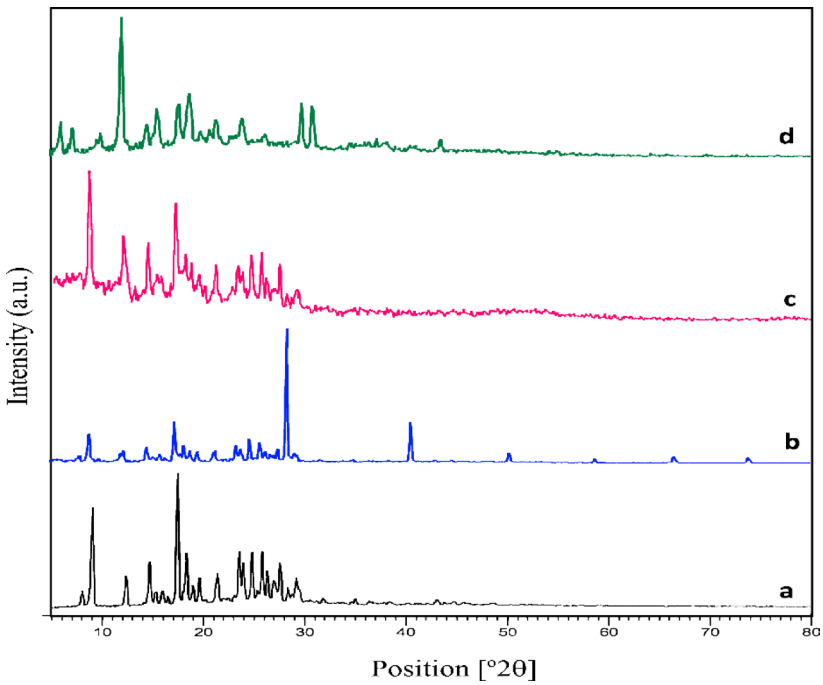


Fig. 8. XRD patterns of **a** curcumin, **b** K-CD-MOF@Cur, **c** Fe-CD-MOF@Cur, and **d** Fe/K-CD-MOF@Cur.

peaks at regions of 1500 and 1270 cm^{-1} in both monometallic and bimetallic MOFs are related to the stretching vibration of the C=C and C-O bonds in curcumin over MOFs, respectively. The peak at 2920 cm^{-1} is related to γ-CD, and it remains stable in X-MOF@Cur. These FT-IR spectral features indicated the successful loading of curcumin over both monometallic and bimetallic coordination networks. The XRD pattern of curcumin, K-MOF@Cur, Fe-MOF@Cur, and Fe/K-MOF@Cur is depicted in Fig. 8a, b and c, and 8d, respectively. The broad feature centered near 30° in Fig. 8b (K-MOF@Cur) corresponds to the amorphous curcumin fraction, which is less pronounced in the bimetallic system (Fig. 8d), suggesting more uniform dispersion of curcumin

within the Fe/K-CD-MOF matrix. Both mono and bi-metallic forms of metal-organic frameworks (MOFs) show altered patterns when curcumin is present on/in them as evidenced by the characteristic bands attributed to curcumin in the Fourier Transform Infrared (FT-IR) spectra as well as the change in intensity and width of peaks (broadening) and the structure of the frame remains intact, confirming the formation of curcumin incorporated into the carrier matrices.

pH-dependent release behavior

The release behavior of curcumin from the synthesized carriers was investigated under acidic (pH 2.0) and neutral (pH 7.4) conditions to simulate gastric and physiological environments. The release profiles demonstrate a clear pH-dependent behavior for all carriers, indicating their sensitivity to the surrounding medium. At pH 7.4, curcumin exhibited higher adsorption and a more controlled release compared to acidic conditions, where faster release was observed (Fig. 9).

At pH 2.0, the highest release rate was observed for K-MOF, followed by Fe/K-MOF and Fe-MOF. This behavior can be attributed to the relatively weaker K–O coordination bonds, which are more susceptible to proton-induced framework relaxation under acidic conditions, facilitating curcumin release. In contrast, stronger Fe–O coordination interactions result in a more rigid framework, thereby restricting curcumin release. Under neutral conditions (pH 7.4), the Fe/K-MOF exhibited the highest release efficiency, followed by Fe-MOF and K-MOF. The superior performance of the bimetallic system is attributed to its smaller particle size, uniform metal distribution, and more accessible coordination environment, as confirmed by SEM, TEM, and EDS analyses.

Release kinetics modeling

The release kinetics of curcumin (Figs. 10 and 11) were analyzed using the Freundlich, Elovich, and Ritger–Peppas models[42]. Among these kinetic models, the Ritger–Peppas model exhibited the highest correlation coefficients (R^2=0.95), indicating the best agreement with the experimental release data and providing a more accurate description of the release behavior compared to the other models[43].

The kinetic analysis highlights the important role of metal incorporation in regulating curcumin loading and release behavior, particularly in the bimetallic Fe/K-MOF system. The Fe/K-MOF demonstrated a well-balanced and pH-responsive release profile, which is a critical requirement for effective delivery applications.

Furthermore, the release exponent (n = 0.4–0.5) values derived from the Ritger–Peppas model suggest that curcumin release follows an anomalous transport mechanism, governed by a combination of diffusion and matrix relaxation processes. This behavior is especially pronounced under acidic conditions, where partial framework relaxation facilitates controlled release. These findings confirm that the bimetallic Fe/K coordination environment plays a key role in modulating release kinetics and enhancing the performance of γ-CD-based MOFs as curcumin carriers. This anomalous release behavior is further supported by BET and SEM analyses, which revealed an increased specific surface area, hierarchical porosity, and reduced particle size for the Fe/K-MOF, collectively facilitating enhanced diffusion pathways and matrix relaxation during curcumin release.

Conclusions

Mono- and bimetallic γ-cyclodextrin-based metal–organic frameworks were successfully synthesized via a modified vapor diffusion approach to evaluate the influence of heterometallic coordination on framework structure and functionality. Structural analyses confirmed that concurrent incorporation of Fe^{3+} and K^{+} ions preserves the intrinsic crystalline architecture of the γ-cyclodextrin network while enhancing long-range ordering, as evidenced by low-angle X-ray diffraction. Compared with monometallic analogues, the bimetallic

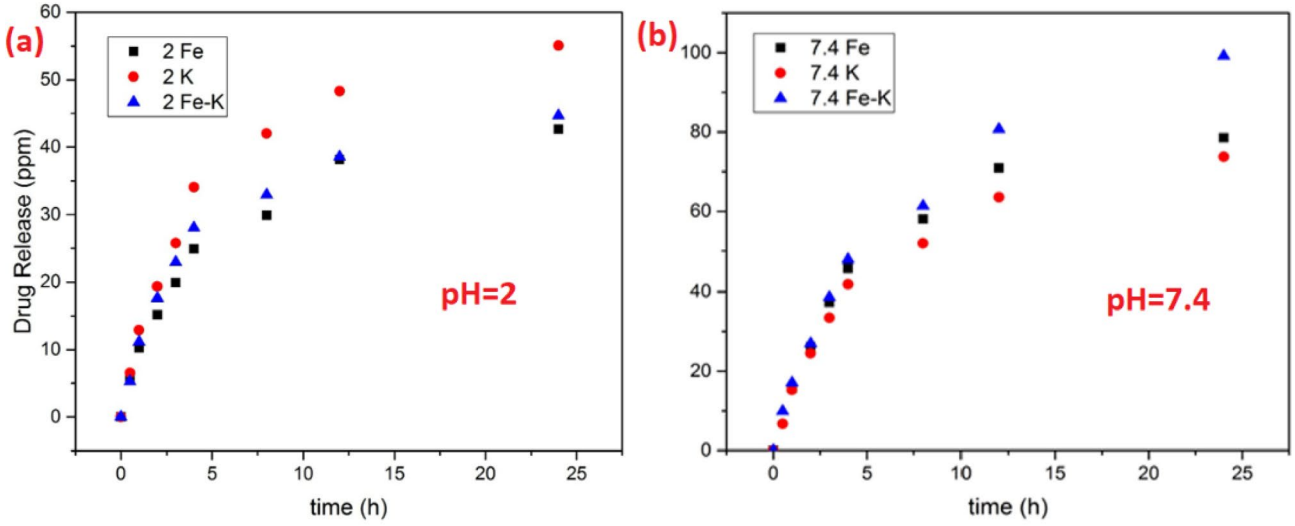
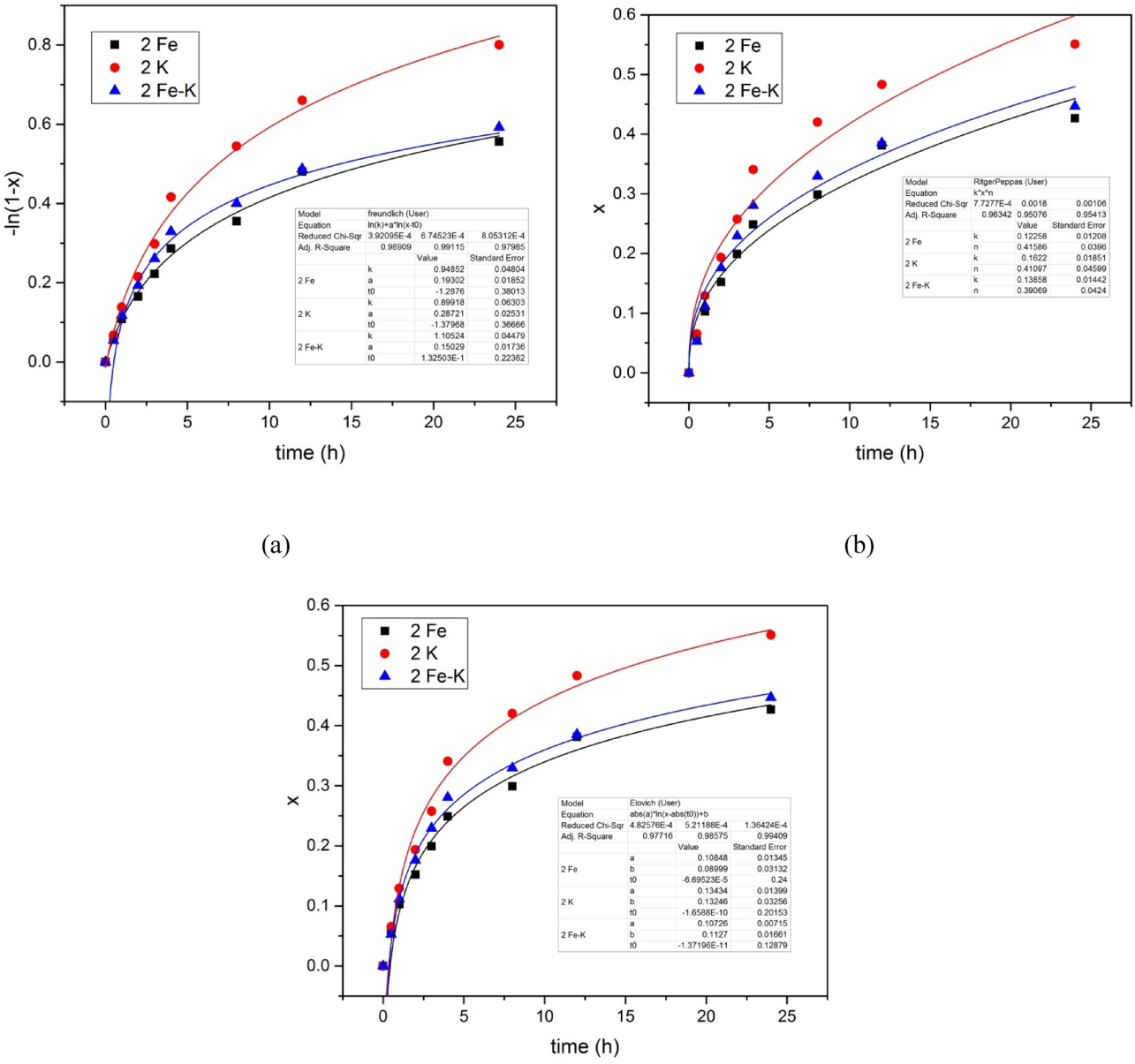


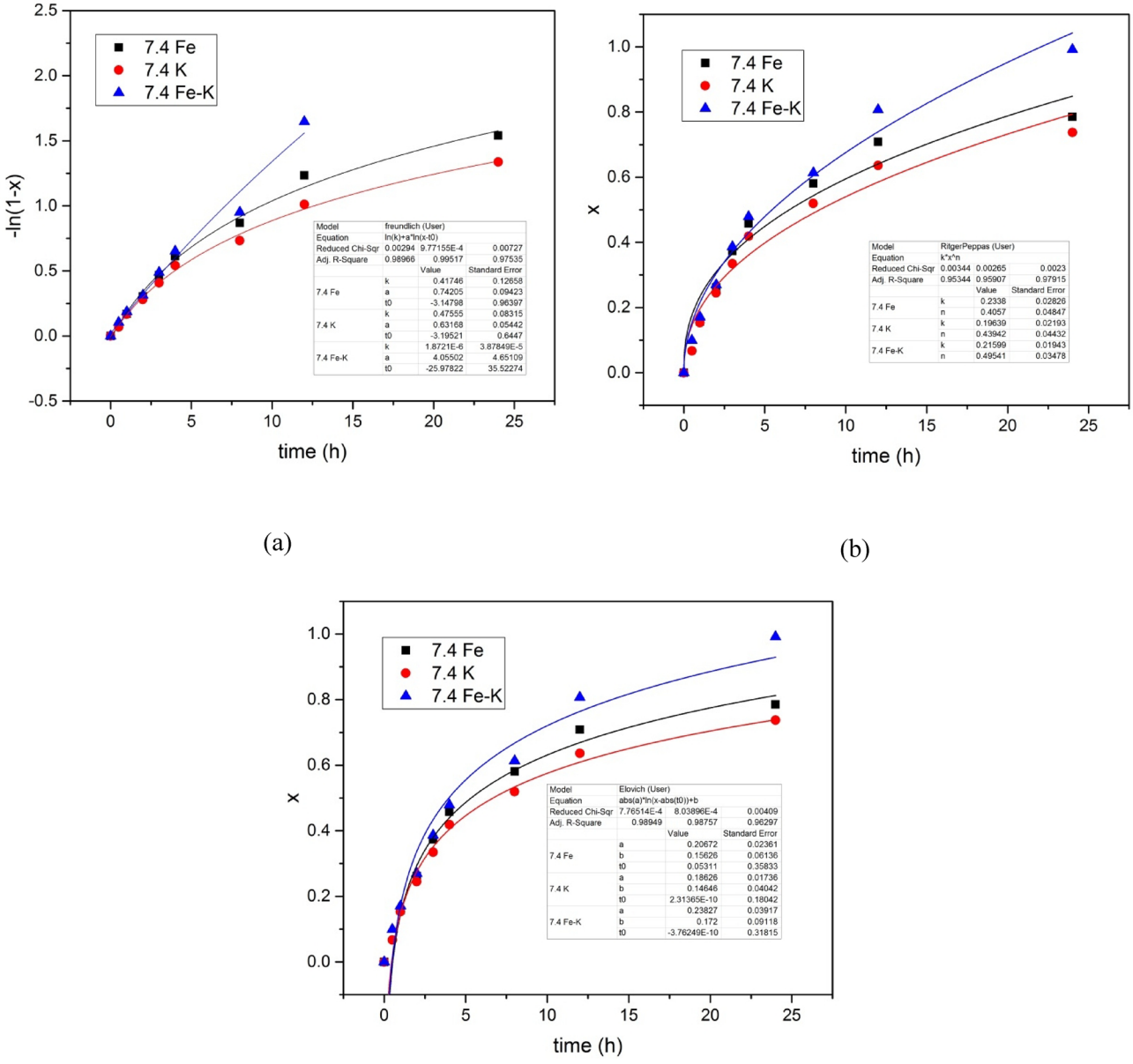
Fig. 9. Effect of pH on the release behavior of curcumin from CD-MOF host systems.



(a) (b) (c)

Fig. 10. Release kinetics of curcumin from CD-MOF systems at pH 2.0 fitted with **a** Freundlich, **b** Ritger–Peppas, and **c** Elovich models.

Fe/K-γ-CD-MOF exhibited increased crystallinity, more uniform nanoscale morphology, and higher accessible surface area, indicating that dual-metal coordination modifies crosslinking density and framework organization without disrupting the carbohydrate scaffold. Host–guest studies using curcumin as a model hydrophobic compound demonstrated improved encapsulation efficiency and controlled release behavior in the bimetallic system, particularly under physiological conditions (pH 7.4). The enhanced performance is attributed to synergistic coordination effects arising from the combined presence of monovalent and trivalent metal centers, which influence pore accessibility and framework–guest interactions. Release kinetics analysis indicated anomalous transport behavior governed by coupled diffusion and matrix relaxation processes, confirming that structural modulation directly impacts guest mobility within the porous network. Overall, this study establishes a clear correlation between heterometallic coordination environment, structural ordering, and functional host–guest performance in γ-cyclodextrin MOFs. We acknowledge that systematic variation of the Fe/K feed ratio was beyond the scope of this initial proof-of-concept study. Preliminary experiments with higher Fe/K ratios resulted in reduced crystallinity and framework collapse, suggesting that the 1:4.5 Fe/K ratio (relative to the 0.2 mmol γ-CD) represents a near-optimal composition under our synthesis conditions. Future work



(a) (b)

(c)

Fig. 11. Release kinetics of curcumin from CD-MOF systems at pH 7.4 fitted with **a** Freundlich, **b** Ritger–Peppas, and **c** Elovich models.

will systematically optimize the metal stoichiometry to establish structure–property correlations across a wider compositional range. The current results demonstrate that bimetallic Fe/K modulation provides a rational strategy for tuning carbohydrate-based coordination frameworks. Given the mild synthesis conditions and the observed pH-responsive release behavior, these materials represent a versatile platform for further development of bio-derived porous carriers and related controlled molecular delivery systems.

Data availability

No datasets were generated or analysed during the current study.

Received: 25 February 2026; Accepted: 17 April 2026
Published online: 22 April 2026

References

1. Kumar, A. et al. A porous metal–organic framework (Pd-MOF) as an efficient and recyclable catalyst for the C–O cross-coupling reactions. *Sci. Rep.* **15**, 13070. https://doi.org/10.1038/s41598-025-97157-2 (2025).
2. Li, W. et al. Zinc(II) organic framework based bifunctional biomarker sensor for efficient detection of urinary 5-Hydroxyindoleacetic acid and serum 3-Nitrotyrosine. *Spectrochim Acta Part. Mol. Biomol. Spectrosc.* **329**, 125610. https://doi.org/10.1016/j.saa.2024.125610 (2025).
3. Joseph, N. et al. Synthesis and characterization of CaSr-Metal Organic Frameworks for biodegradable orthopedic applications. *Sci. Rep.* **9**, 13024. https://doi.org/10.1038/s41598-019-49536-9 (2019).
4. Li, C., Fan, L., Hu, T., Qin, Q.-P. & Zhang, X. Two-dimensional nanoporous {Tb2}–organic framework with acid–base for CO2-epoxide cycloaddition and deacetalization–knoevenagel condensation. *ACS Appl. Nano Mater.* **8**, 15288–15298. https://doi.org/10.1021/acsanm.5c02665 (2025).
5. Shamloo, A. et al. In-silico study of drug delivery to atherosclerosis in the human carotid artery using metal–organic frameworks based on adhesion of nanocarriers. *Sci. Rep.* **13**, 21481. https://doi.org/10.1038/s41598-023-48803-0 (2023).
6. Fytory, M. et al. Dual-ligated metal organic framework as novel multifunctional nanovehicle for targeted drug delivery for hepatic cancer treatment. *Sci. Rep.* **11**, 19808. https://doi.org/10.1038/s41598-021-99407-5 (2021).
7. Li, X. et al. New insights into the degradation mechanism of metal-organic frameworks drug carriers. *Sci. Rep.* **7**, 13142. https://doi.org/10.1038/s41598-017-13323-1 (2017).
8. Zorlu, T., Hetey, D., Reithofer, M. R. & Chin, J. M. Physicochemical methods for the structuring and assembly of MOF crystals. *Acc. Chem. Res.* **57**, 2105–2116 (2024).
9. Cook, T. R., Zheng, Y-R. & Stang, P. J. Metal–organic frameworks and self-assembled supramolecular coordination complexes: comparing and contrasting the design, synthesis, and functionality of metal–organic materials. *Chem. Rev.* **113**, 734–777 (2013).
10. Liu, J., Li, Y. & Lou, Z. Recent advancements in MOF/biomass and Bio-MOF multifunctional materials: A review. *Sustainability* **14**, 5768 (2022).
11. Roy, I. & Stoddart, J. F. Cyclodextrin metal–organic frameworks and their applications. *Acc. Chem. Res.* **54**, 1440–1453 (2021).
12. Hamedi, A., Anceschi, A., Patrucco, A. & Hasanzadeh, M. A γ-cyclodextrin-based metal–organic framework (γ-CD-MOF): A review of recent advances for drug delivery application. *J. Drug Target.* **30**, 381–393 (2022).
13. Shen, D. et al. Epitaxial growth of γ-cyclodextrin-containing metal–organic frameworks based on a host–guest strategy. *J. Am. Chem. Soc.* **140**, 11402–11407 (2018).
14. Ghorbani-Choghamarani, A., Taherinia, Z. & Mohammadi, M. Facile synthesis of Fe3O4@ GlcA@ Ni-MOF composites as environmentally green catalyst in organic reactions. *Environ. Technol. Innov.* **24**, 102050 (2021).
15. Li, H. et al. Porous metal-organic frameworks for gas storage and separation: Status and challenges. *EnergyChem* **1**, 100006 (2019).
16. Lu, K., Aung, T., Guo, N., Weichselbaum, R. & Lin, W. Nanoscale metal–organic frameworks for therapeutic, imaging, and sensing applications. *Adv. Mater.* **30**, 1707634 (2018).
17. Rocío-Bautista, P., Taima-Mancera, I., Pasán, J. & Pino, V. Metal-organic frameworks in green analytical chemistry. *Separations* **6**, 33 (2019).
18. Sharanyakanth, P. S. & Radhakrishnan, M. Synthesis of metal-organic frameworks (MOFs) and its application in food packaging: A critical review. *Trends Food Sci. Technol.* **104**, 102–116 (2020).
19. Zhou, H-C., Long, J. R. & Yaghi, O. M. Introduction to metal–organic frameworks. *Chem. Rev.* **112**, 673–674 (2012).
20. Pan, X. et al. Effect of potassium salts on the structure of γ-cyclodextrin MOF and the encapsulation properties with thymol. *J. Sci. Food Agric.* **102**, 6387–6396 (2022).
21. Jiang, W. et al. Preparation of two metal organic frameworks (K-β-CD-MOFs and Cs-β-CD-MOFs) and the adsorption research of myricetin. *Polyhedron* **196**, 114983 (2021).
22. Patel, H. A. et al. Noninvasive substitution of K+ sites in cyclodextrin metal–organic frameworks by Li+ ions. *J. Am. Chem. Soc.* **139**, 11020–11023 (2017).
23. Khan, M. S. & Shahid, M. Synthesis of metal-organic frameworks (MOFs): routes to various MOF topologies, morphologies, and composites. In *Electrochemical Applications of Metal-Organic Frameworks*, 17–35 (Elsevier, 2022).
24. Stock, N. & Biswas, S. Synthesis of metal-organic frameworks (MOFs): routes to various MOF topologies, morphologies, and composites. *Chem. Rev.* **112**, 933–969 (2012).
25. Anand, R. et al. Host–guest interactions in Fe (III)-trimesate MOF nanoparticles loaded with doxorubicin. *J. Phys. Chem. B.* **118**, 8532–8539 (2014).
26. Tian, S. et al. Highly efficient removal of both cationic and anionic dyes from wastewater with a water-stable and eco-friendly Fe-MOF via host-guest encapsulation. *J. Clean. Prod.* **239**, 117767 (2019).
27. Liu, X. et al. Iron-based metal–organic frameworks in drug delivery and biomedicine. *ACS Appl. Mater. Interfaces.* **13**, 9643–9655 (2021).
28. Brozek, C. K. & Dincă, M. Ti3+-, V2+/3+-, Cr2+/3+-, Mn2+-, and Fe2+-substituted MOF-5 and redox reactivity in Cr-and Fe-MOF-5. *J. Am. Chem. Soc.* **135**, 12886–12891 (2013).
29. Kang, L. et al. Preparation technology and preservation mechanism of γ-CD-MOFs biaological packaging film loaded with curcumin. *Food Chem.* **420**, 136142 (2023).
30. Sha, L. et al. Genipin-enriched chitosan-Zein nanoparticles for improved curcumin encapsulation. *Int. J. Biol. Macromol.* **288**, 138555. https://doi.org/10.1016/j.ijbiomac.2024.138555 (2025).
31. Nie, M. et al. Optimizing enzymatic treatment of porous waxy rice starch for dual-encapsulation with chitosan: enhancing apigenin delivery. *Int. J. Biol. Macromol.* **347**, 150710. https://doi.org/10.1016/j.ijbiomac.2026.150710 (2026).
32. Farshchi-Andisi, A. et al. Hydrogel composite for curcumin encapsulation using whey protein isolate and arabinoxylan extracted from sesame hull waste. *Int. J. Biol. Macromol.* **319**, 145575. https://doi.org/10.1016/j.ijbiomac.2025.145575 (2025).
33. Yang, R. et al. A pH-sensitive dual-encapsulating delivery system: Chitosan-alginate hydrogels trapping glycyrrhizic acid/curcumin micelles for synergistic ulcerative colitis. *Int. J. Biol. Macromol.* **339**, 149975. https://doi.org/10.1016/j.ijbiomac.2025.149975 (2026).
34. Horcajada, P. et al. Metal–organic frameworks in biomedicine. *Chem. Rev.* **112**, 1232–1268 (2012).
35. Krūkle-Bērziņa, K. & Mishnev, A. Never-ending story: New cyclodextrin-based metal–organic framework crystal structures obtained using different crystallization methods. *ACS Omega* **8**, 48221–48232. https://doi.org/10.1021/acsomega.3c07429 (2023).
36. Hoskins, B. F. & Robson, R. Infinite polymeric frameworks consisting of three dimensionally linked rod-like segments. *J. Am. Chem. Soc.* **111**, 5962–5964 (1989).
37. Maity, R. et al. Aqueous-phase differentiation and speciation of Fe3 + and Fe2 + using water-stable photoluminescent lanthanide-based metal–organic framework. *ACS Appl. Nano Mater.* **2**, 5169–5178 (2019).
38. Xiong, Y. Y. et al. MOF catalysis of FeII-to-FeIII reaction for an ultrafast and one-step generation of the Fe2O3@MOF composite and uranium(vi) reduction by iron(ii) under ambient conditions. *Chem. Commun.* **52**, 9538–9541. https://doi.org/10.1039/C6CC04597A (2016).
39. Yamaguchi, T. et al. NKX2-1/TITF1/TTF-1-Induced ROR1 is required to sustain EGFR survival signaling in lung adenocarcinoma. *Cancer Cell.* **21**, 348–361 (2012).
40. Smaldone, R. A. et al. Metal–organic frameworks from edible natural products. *Angew Chemie Int. Ed.* **49**, 8630–8634. https://doi.org/10.1002/anie.201002343 (2010).
41. Hernandez, J. G. & Friščić, T. Metal-catalyzed organic reactions using mechanochemistry. *Tetrahedron Lett.* **56**, 4253–4265 (2015).

42. Chen, Y. et al. Development of iron-modified soybean protein nanoparticles for the enrichment and controlled release of flavonoid compounds in sea buckthorn fruit residue extract. *Food Biosci.* 107585 (2025).
43. Sulttan, S. & Rohani, S. Controlled drug release of smart magnetic self-assembled micelle, kinetics and transport mechanisms. *J. Pharm. Sci.* **111**, 2378–2388 (2022).

Author contributions

Asma Sadeghi: Methodology; Investigation; Formal analysis; Data curation; Visualization; Writing – original draftHamidreza Farnoush: Conceptualization; Methodology; Investigation; Data curation; Writing – review & editing; SupervisionJavad Safaei-ghomi: Conceptualization; Methodology; Investigation; Writing – review & editing; SupervisionHourieh Sadat Oboudatian: Methodology; Investigation; Formal analysis; Data curation; Visualization; Writing – original draft.

Funding

The authors declare no conflicts of interest. This research received no specific grant from any funding agency in the public, commercial, or not-for-profit sectors.

Declarations

Competing interests

The authors declare no competing interests.

Additional information

Supplementary Information The online version contains supplementary material available at https://doi.org/10.1038/s41598-026-50037-9.

Correspondence and requests for materials should be addressed to H.F. or J.S.-g.

Reprints and permissions information is available at www.nature.com/reprints.

Publisher's note Springer Nature remains neutral with regard to jurisdictional claims in published maps and institutional affiliations.

Open Access This article is licensed under a Creative Commons Attribution-NonCommercial-NoDerivatives 4.0 International License, which permits any non-commercial use, sharing, distribution and reproduction in any medium or format, as long as you give appropriate credit to the original author(s) and the source, provide a link to the Creative Commons licence, and indicate if you modified the licensed material. You do not have permission under this licence to share adapted material derived from this article or parts of it. The images or other third party material in this article are included in the article's Creative Commons licence, unless indicated otherwise in a credit line to the material. If material is not included in the article's Creative Commons licence and your intended use is not permitted by statutory regulation or exceeds the permitted use, you will need to obtain permission directly from the copyright holder. To view a copy of this licence, visit http://creativecommons.org/licenses/by-nc-nd/4.0/.

© The Author(s) 2026